

# Time evolution of the one-dimensional Jaynes-Cummings-Hubbard Hamiltonian

M.I. Makin,<sup>1</sup> Jared H. Cole,<sup>2</sup> Charles D. Hill,<sup>1</sup> Andrew D. Greentree,<sup>1</sup> and Lloyd C. L. Hollenberg<sup>1</sup>

<sup>1</sup>*Center for Quantum Computer Technology, School of Physics,  
The University of Melbourne, Victoria 3010, Australia*

<sup>2</sup>*Institut für Theoretische Festkörperphysik and DFG-Center for Functional  
Nanostructures (CFN), Universität Karlsruhe, 76128, Germany*

The Jaynes-Cummings-Hubbard (JCH) system describes a network of single-mode photonic cavities connected via evanescent coupling. Each cavity contains a single two level system which can be tuned in resonance with the cavity. Here we explore the behavior of single excitations (where an excitation can be either photonic or atomic) in the linear JCH system, which describes a coupled cavity waveguide. We use direct, analytic diagonalization of the Hamiltonian to study cases where inter-cavity coupling is either uniform or varies parabolically along the chain. Both excitations located in a single cavity, as well as one excitation as a Gaussian pulse spread over many cavities, are investigated as initial states. We predict unusual behavior of this system in the time domain, including slower than expected propagation of the excitation, and also splitting of the excitation into two distinct pulses, which travel at distinct speeds. In certain limits, we show that the JCH system mimics two Heisenberg spin chains.

## I. INTRODUCTION

The realization of condensed matter models using non-traditional controllable systems has been an active topic of recent research. This is best exemplified by the work on cold atom quantum simulators [1, 2]. However the possibility of quantum optical simulators for condensed matter models has emerged. While finding links and analogies between different subfields of physics is interesting in its own right, of particular interest are effects that are difficult or impossible to observe in more conventional physical systems.

There are a number of recent proposals [3, 4, 5, 6, 7, 8, 9, 10] for constructing quantum optical condensed matter simulators. These use coupled cavity structures where confined photons are induced to interact via their coupling to embedded two-state systems. Possible two-state systems include color centers [4], quantum dots [11, 12], superconducting strip-line resonators [13, 14, 15], or coupled Rubidium microcavities [16].

In such systems, it should be possible to observe many-body effects such as quantum phase transitions where the particles of interest are photons (rather than electrons) and therefore can be readily injected, confined and observed individually. While many-body effects in the thermodynamic limit require a large number of cavities and/or photons (often solved in the mean field limit), it is quite clear that early experiments will be limited in both overall structure size and system controllability. It is therefore of interest to determine what (if any) effects can be observed in the few cavity/few excitation limit (where an excitation can either be photonic or atomic) [8, 17, 18, 19]. Importantly, the complex interactions between atomic and photonic components produce a variety of effects. Solitonic behavior has been predicted in the 1D coupled cavity wave guide realizations of the Dicke model [20] and the XXZ model in the presence of a tilted magnetic field [21]. If one is considering, for example, the type of localized/delocalized behavior typically

found in strongly interacting systems, it is of vital importance not to be distracted by the background effects which come from the delocalized behaviour of photons themselves. For this reason, a detailed understanding of the single-particle dynamics is paramount.

Here we investigate the time evolution of a one dimensional coupled cavity waveguide [22] described by the Jaynes-Cummings-Hubbard (JCH) model [4]. In the single excitation subspace we diagonalize the JCH Hamiltonian exactly and consider the dependence of this system on three parameters: atom-cavity detuning, atom-photon coupling and coupling between cavities. We then investigate limits in which localized and delocalized behaviour can be seen. In this paper, we refer to the propagation of photonic or atomic excitations as the photonic and atomic components, or modes, respectively (in the atomic case, the atoms remain stationary whilst the excitation passes through). In particular we focus on three limits. Firstly, the limit where the atom-cavity detuning is zero and the coupling strength between cavities is much less than the photonic cavity-atomic coupling. In this limit, the propagation dynamics of the atomic and photonic components are identical; we find they propagate as a pulse travelling back and forth along the line of cavities. Secondly, we study the limit where photon hopping dominates all other parameters of the system. In this limit, the atomic component does not move, while the photonic component propagates. Thirdly, we study the limit where the atom-cavity detuning is much larger than all other energy scales of the system. In this limit the atomic and photonic modes travel at two different speeds. In these three limits we compare the behaviour with that of two uncoupled Heisenberg spin chains [5, 23, 24], in the one-excitation case.

We discuss the JCH model and the uniform coupling case in Sec. II. We then continue with dispersion-free pulses using parabolic coupling, Sec. III, and initial Gaussian pulses, Sec. IV. In Sec. V we discuss the limit of large atom-cavity detuning, in this limit the atomic and

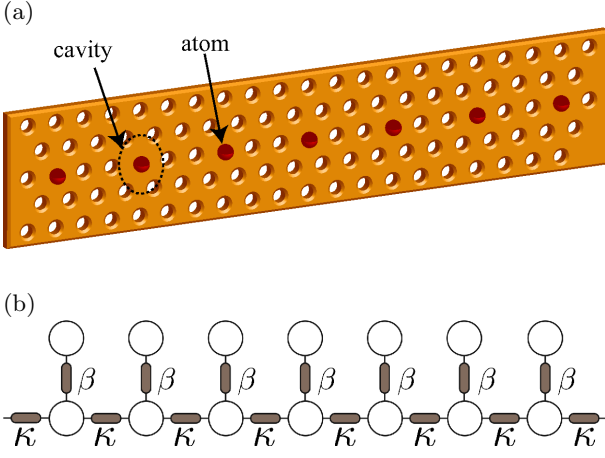


FIG. 1: (Color online) Visualizations of a 1D JCH system. Fig. (a) shows an example of a coupled cavity waveguide in a photonic crystal. A lattice of holes in the membrane provide variations in refractive index, hence trapping photons of a given frequency. The red spheres indicate two-level systems, these are placed at sites without holes, called defects, which form photonic cavities. Fig. (b) is a visualization of a portion of a JCH chain as logical elements. The bottom row of circles indicate the photonic cavities, linked together by the hopping rate  $\kappa$ . The top row of circles indicate the atoms, linked back to each photonic cavity by the coupling strength  $\beta$  [defined in Eq. (1)].

photonic modes travel at two distinct speeds.

## II. UNIFORM COUPLING

The JCH Hamiltonian ( $\mathcal{H}^{\text{JCH}}$ ) describes a system of  $N$  cavities linked via photon hopping under the tight-binding approximation [4, 5, 19]. A possible arrangement and schematic showing the couplings is shown in Fig. (1). The Hamiltonian is

$$\mathcal{H}^{\text{JCH}} = \sum_{i=1}^N \mathcal{H}_i^{\text{JC}} - \kappa \sum_{i,j=1}^N A_{ij} a_i^\dagger a_j, \quad (1)$$

where  $\kappa$  is the inter-cavity coupling, and  $A$  is the adjacency matrix, which is defined according to the geometry and boundary conditions of the system. Using the geometry as implied by Fig. (1)(a), that is, one spatial dimension with hard wall boundary conditions,  $A$  is given by

$$A_{ij} = \begin{cases} 1, & \text{if } |i-j| = 1 \\ 0, & \text{otherwise} \end{cases}. \quad (2)$$

The Jaynes-Cummings Hamiltonian  $\mathcal{H}^{\text{JC}}$  [25] describes a single atom-cavity system. It can be written

$$\mathcal{H}_i^{\text{JC}} = \epsilon_i \sigma_i^+ \sigma_i^- + \omega_i a_i^\dagger a_i + \beta_i (\sigma_i^+ a_i + \sigma_i^- a_i^\dagger), \quad (3)$$

where  $a_i^\dagger$  ( $a_i$ ) and  $\sigma_i^+$  ( $\sigma_i^-$ ) are the photonic and atomic raising (lowering) operators respectively, and  $\hbar = 1$ . In cavity  $i$ , the energy of the atom is given by  $\epsilon_i$ , the cavity resonance by  $\omega_i$ , and the cavity-atom coupling by  $\beta_i$ .

The single cavity *bare basis* consists of states of the form  $|s, n\rangle$ , where  $s \in \{g, e\}$  represents the two-level atom in the ground or excited state, and  $n$  is a non-negative integer, representing the number of photons in the cavity. The  $N$  cavity bare basis simply consists of the tensor product of  $N$  such single cavity bare bases.

The single cavity *dressed basis* consists of the state  $|g, 0\rangle$  (this state is a member of both the bare and dressed bases) and states of the form  $|\pm, n\rangle$ , where  $n$  is the number of excitations (photonic or atomic) in the cavity. They are energy eigenstates of the Jaynes-Cummings Hamiltonian, and are related to the single cavity bare basis states by

$$|\pm, n\rangle = \frac{\beta\sqrt{n}|g, n\rangle + [-(\Delta/2) \pm \chi(n)]|e, n-1\rangle}{\sqrt{2\chi^2(n) \mp \chi(n)\Delta}} \quad \forall n \geq 1, \quad (4)$$

where  $\Delta = \omega - \epsilon$  is the detuning, and we have used the generalized Rabi frequency

$$\chi(n) = \sqrt{n\beta^2 + \Delta^2/4} \quad \forall n \geq 1. \quad (5)$$

Consider a restricted basis of the full  $N$  cavity bare basis, consisting only of basis states that contain one excitation (atomic or photonic) in the whole system: the one excitation subspace. The total number of excitations in the JCH system is conserved, hence this is a restriction, not an approximation. We consider the case where all cavities are equal, hence  $\epsilon_i = \epsilon, \omega_i = \omega, \beta_i = \beta$  for all  $i = 1, \dots, N$ . We write the restricted one excitation basis as  $|Q\rangle \otimes |g, 1\rangle$  ( $|Q\rangle \otimes |e, 0\rangle$ ), where  $Q \in \{1, \dots, N\}$ , to mean a photonic excitation  $|g, 1\rangle$  (atomic excitation  $|e, 0\rangle$ ) at cavity number,  $Q$ , and  $|g, 0\rangle$  at every other cavity position. The states  $|Q\rangle$  form a valid Hilbert space. In this restricted basis and under these conditions, the Hamiltonian (1) is greatly simplified, and can be represented

$$\mathcal{H}_{\text{lexc}}^{\text{JCH}} = \frac{\Delta}{2} I_N \otimes Z + \beta I_N \otimes X - \kappa A \otimes \frac{I_2 + Z}{2}, \quad (6)$$

where  $I_m$  is the  $m \times m$  identity matrix,  $X$  and  $Z$  are the usual Pauli matrices acting on the atom-photon cavity subspace. The operator  $A$  in matrix form is given by the adjacency matrix of the connectivity graph, for example that given in Eq. (2). In this form, the first and second terms affect only the atomic/photonic modes locally, but do not move the excitation to any other cavity. The first term describes the detuning and the second term the coupling between photonic and atomic excitation modes. The third term describes photonic coupling between cavities.

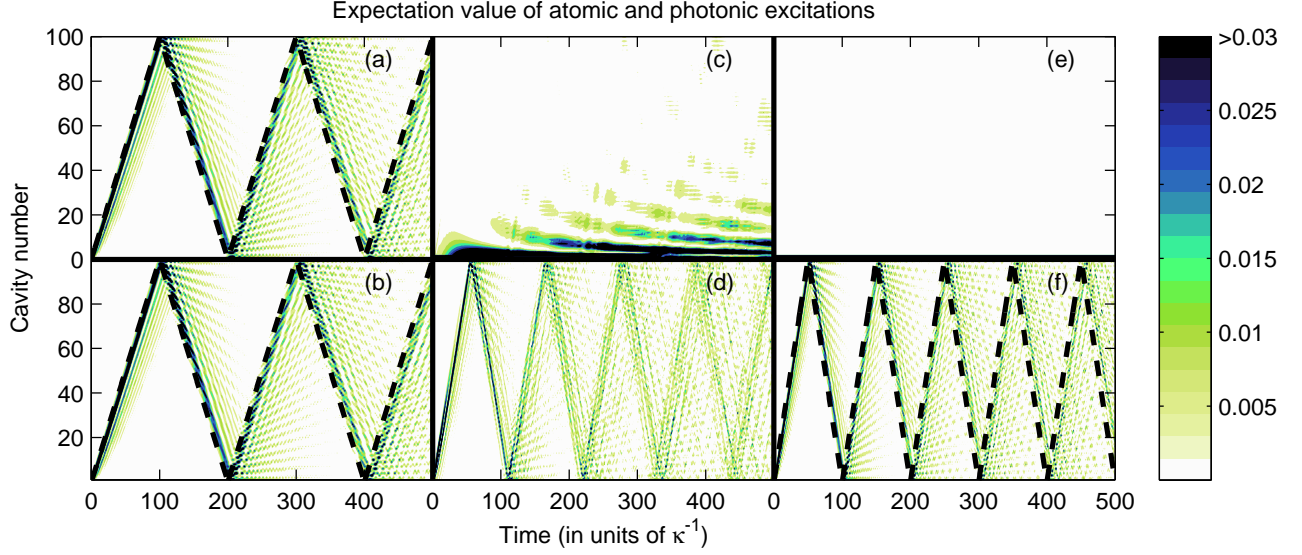


FIG. 2: (Color online) Space-time diagrams for evolution of an excitation  $(|1\rangle \otimes (|g, 1\rangle + |e, 0\rangle)/\sqrt{2})$  along a chain of 100 JC cavities for three different parameter regimes. In each case, we plot the probability of occupation of a particular cavity (vertical axis) as a function of time (horizontal axis) for the system initialized in an even superposition of the atomic and photonic mode of the first cavity. The upper three plots show the population of the atomic components whereas the lower three plots are the photonic components. The ratio of cavity-cavity coupling to atom-photon coupling varies from left to right, with (a) and (b)  $\kappa/\beta = 10^{-3}$ , (c) and (d)  $\kappa/\beta = 10$  and (e) and (f)  $\kappa/\beta = 10^3$ . In plots (a), (b) and (f), the dashed lines represent  $Q_\Lambda$ , as given in Eq. (15).

By diagonalizing  $A$  the whole JCH Hamiltonian restricted to one excitation can be diagonalized. We now solve for the 1D chain with hard wall boundary conditions. The eigenvectors of the  $A$  matrix given in Eq. (2) are [26]

$$|k\rangle = \frac{\sqrt{2}(-1)^k \sin\left(\frac{Nk\pi}{N+1}\right)}{\sqrt{N+1} \sin\left(\frac{k\pi}{N+1}\right)} \sum_{Q=1}^N \sin\left(\frac{Qk\pi}{N+1}\right) |Q\rangle, \quad (7)$$

where  $k = 1, \dots, N$ .

We now wish to obtain the energy eigenstates and energy eigenvalues for the entire one excitation subspace. For a linear chain of cavities the Hamiltonian  $\mathcal{H}_{\text{1exc}}^{\text{JCH}}$  can be expressed in the basis  $\{|k\rangle \otimes |g, 1\rangle, |k\rangle \otimes |e, 0\rangle\}$ ,  $k = 1, \dots, N$  as a block diagonal matrix, in which the  $k$ th block appears as

$$\mathcal{H}_{\text{1exc}}^{\text{JCH}}(k) = \begin{pmatrix} \Delta/2 + 2\kappa \cos[k\pi/(N+1)] & \beta \\ \beta & -\Delta/2 \end{pmatrix}. \quad (8)$$

The eigenvalues of the full Hamiltonian, from Eq. (6), are

$$E_{\pm}^k = \kappa \cos\left(\frac{k\pi}{N+1}\right) \pm \sqrt{\left[\frac{\Delta}{2} + \kappa \cos\left(\frac{k\pi}{N+1}\right)\right]^2 + \beta^2}, \quad (9)$$

where the second term of this appears very similar to the Rabi frequency  $\chi(1)$ , Eq. (5), with the detuning  $\Delta$  shifted by the cosine term. These eigenvalues have corresponding eigenvectors

$$|\pm, k\rangle = \left[ \frac{(\Delta + 2E_{\pm}^k)|e, 0\rangle + 2\beta|g, 1\rangle}{\sqrt{(\Delta + 2E_{\pm}^k)^2 + 4\beta^2}} \right] \otimes |k\rangle. \quad (10)$$

This is an exact diagonalization of the linearly-coupled JCH system in the one excitation subspace. Hence, it is possible to determine analytically, for arbitrary  $N$ , the time-evolution of an arbitrary initial state. In the case with two cavities, i.e.  $N = 2$ , and in appropriate limits to each case, this evolution recovers equations (22), (28) and (29) of Ogden et al. [9]. Specifically, we are interested in plotting the expectation value of both the photonic and atomic excitations in cavity  $j$ , by examining the number operators  $a_j^\dagger a_j$  and  $\sigma_j^+ \sigma_j^-$ .

As a demonstration of the dynamics of the system when on resonance (i.e.  $\Delta = 0$ ), we consider evolution of an excitation initially located in the first cavity in a line of 100 cavities, in an equal superposition of atomic and photonic modes, i.e.

$$|\psi(t=0)\rangle = |1\rangle \otimes (|g, 1\rangle + |e, 0\rangle)/\sqrt{2}, \quad (11)$$

which corresponds to the single cavity energy eigenstate  $|+, 1\rangle$  from Eq. (4) in the case  $\Delta = 0$ . As such, there will

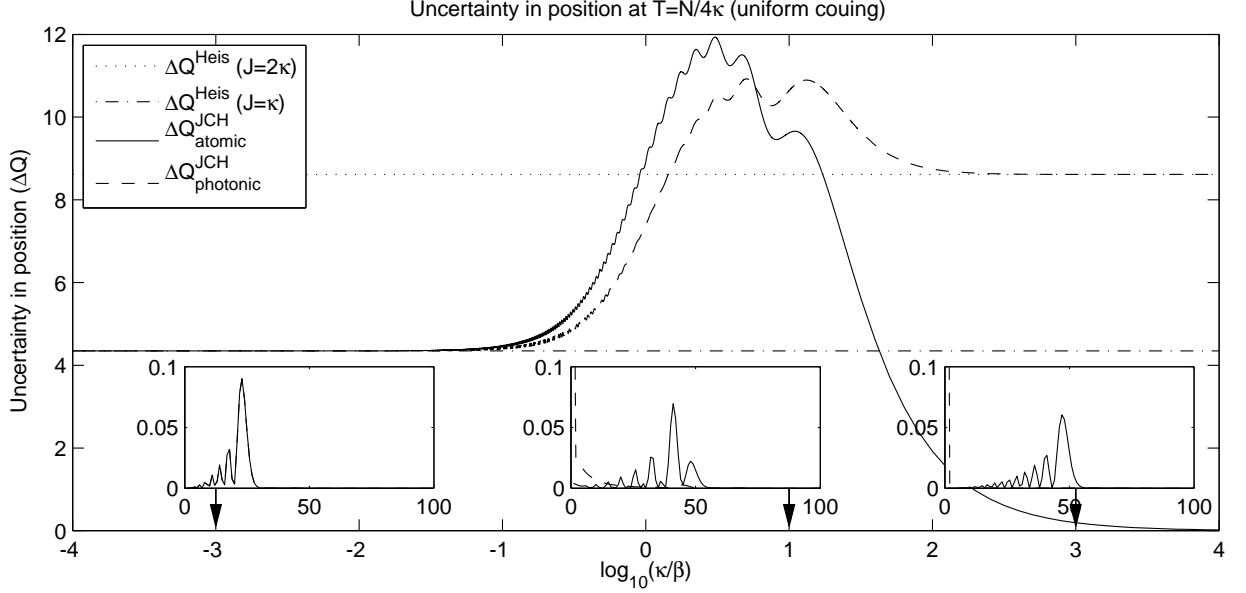


FIG. 3: Dispersion of the wave packet,  $\Delta Q$ , at a fixed point in time, as a function of  $\kappa/\beta$ , with atom-cavity detuning  $\Delta = 0$  and number of cavities  $N = 100$ . The solid (dashed) line shows  $\Delta Q_{\text{atomic}}^{\text{JCH}}$  ( $\Delta Q_{\text{photonic}}^{\text{JCH}}$ ). The dotted (dot-dashed) line shows  $\Delta Q^{\text{Heis}}$  with  $J = 2\kappa$  ( $J = \kappa$ ). The dispersion is measured at a time  $T = N/4\kappa$ , at which point the packet is ‘freely’ evolving along the chain. This point is chosen such that the effects of the hard-wall boundaries can be ignored for both large and small  $\kappa$ . At the left of the plot,  $\kappa/\beta \ll 1$ , and the JCH chain mimics two identical Heisenberg spin chains, an example is shown of this localized behavior in Fig. (2)(a) and (b), where  $\kappa/\beta = 10^{-3}$ . The corresponding spatial profile of the pulse at  $T = N/4\kappa$  is shown in the left inset (the solid line shows the photonic profile and the dashed line shows the atomic profile, in this case they are coincident). At the right of the plot,  $\kappa/\beta \gg 1$ , and the photonic mode of the JCH chain mimics a Heisenberg spin chain, while the atomic mode does not propagate at all. An example of this type of localized behavior is shown in Fig. (2)(e) and (f), where  $\kappa/\beta = 10^3$ , the corresponding profile of the pulse at  $T = N/4\kappa$  is shown in the right inset. In the middle of the plot a travelling excitation shows a large amount of dispersion, an example of this delocalized behavior is shown in Fig. (2)(c) and (d), where  $\kappa/\beta = 10$ , and the corresponding profile at  $T = N/4\kappa$  is shown in the middle inset. The horizontal lines show the dispersion  $\Delta Q^{\text{Heis}}$  of a Heisenberg spin chain with 100 spins after the initial state  $|1\rangle$  evolves until the front of the excitation is half way (dotted line) and quarter way (dot-dashed line) along the excitation chain. The exact correspondence between the Heisenberg and JCH systems is seen in these asymptotic limits.

be no evolution within a cavity, but only evolution between cavities. We solve the evolution exactly, using the usual Schrödinger equation,  $i\partial_t|\psi\rangle = H|\psi\rangle$ . This state also constitutes one of the simplest states to realize experimentally, as the JC resonance can be driven directly by a transverse field. The dispersion and other effects discussed in this paper stem directly from the strong atom-photon interaction via the JC Hamiltonian. If we were to consider a system with vanishing coupling to the atoms ( $\beta = 0$ ), we regain the conventional photon propagation results [17, 18] in which a Gaussian wave propagates smoothly.

We are ultimately interested in the behavior of the system when various energies dominate, such as the atom-photon coupling or the cavity-cavity coupling. For this reason, we will now consider the system in several different limits. When  $\kappa/\beta \ll 1$  and  $\Delta = 0$ , the atomic and photonic modes have identical propagation dynamics. The case  $\kappa/\beta = 10^{-3}$  is shown in Fig. (2)(a) and (b). We may understand the equal propagation because the atom-photon coupling  $\beta$  is much stronger than the

cavity-cavity coupling  $\kappa$ , hence the excitation is free to form the single cavity eigenstate between inter-cavity hops. By shifting to the interaction picture [27], that is  $|\chi\rangle = e^{i\beta I \otimes X t}|\psi\rangle$ , the Hamiltonian Eq. (6) becomes

$$H = -\frac{\kappa}{2}A \otimes I, \quad (12)$$

where the fast rotating terms have been ignored. It is useful at this point to compare with the Hamiltonian that describes the well-known Heisenberg spin chain [28, 29].

$$\begin{aligned} H^{\text{Heis}} &= -J \sum_{n=1}^N \mathbf{S}_n \cdot \mathbf{S}_{n+1} \\ &= -J \sum_{n=1}^N \left[ \frac{1}{2} (S_n^+ S_{n+1}^- + S_n^- S_{n+1}^+) + S_n^z S_{n+1}^z \right]. \end{aligned} \quad (13)$$

The single site basis of this system consists of spins pointing up and down along the direction of the  $z$  axis,  $\{|\uparrow\rangle, |\downarrow\rangle\}$ . The  $N$  site basis comprises of a tensor product

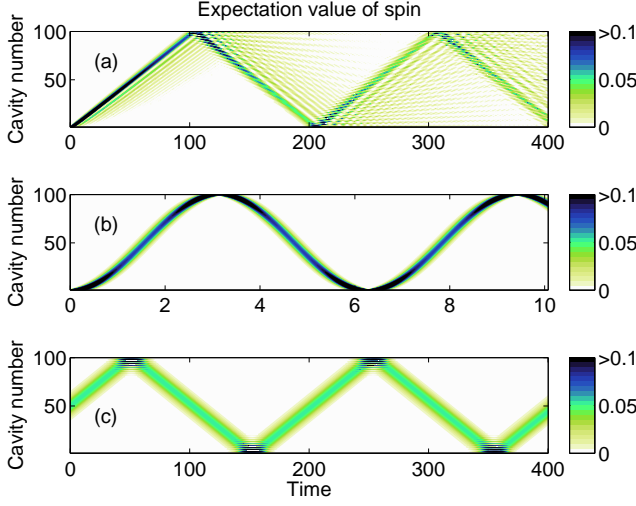


FIG. 4: (Color online) Evolution of a Heisenberg spin chain Hamiltonian [Eq. (14)], with  $J = 1$ . (a) Evolution of  $|1\rangle$  under uniform coupling, note that at first the excitation travels fairly neatly, but both within a single pass, as well as during the reflection, the excitation pulse spreads out. Note the faint lines which are parallel but displaced from the wavefront. These lines are due to the nature of the Heisenberg Hamiltonian. (b) Evolution of  $|1\rangle$  under parabolic coupling, note how the evolution is smooth and repetitive, the excitation travels sinusoidally from one end of the line of spins to the other end and back again, without spreading out. (c) Evolution of a Gaussian pulse as in Eq. (26), with  $Q_c = 50$ ,  $s = 10$ ,  $k = \pi/2$ , with uniform coupling. Note how the evolution is dispersion-free.

of  $N$  such bases. This Hamiltonian also conserves the total spin in the  $z$  direction. So, if we limit the  $N$  site basis to having only one  $|\uparrow\rangle$ , and the rest  $|\downarrow\rangle$ , then the Hamiltonian can be represented in this restricted subspace as (ignoring contributions from the  $S^z$  term, which is largely a phase factor apart from a minor shift at the ends of the chain, this is inconsequential for long chains)

$$H^{\text{Heis}} = -\frac{J}{2}A, \quad (14)$$

where the basis vectors are now  $|1\rangle, |2\rangle, \dots, |N\rangle$ , and  $|Q\rangle$  represents  $|\uparrow\rangle$  at site  $Q$  and  $|\downarrow\rangle$  at every other site, and  $A$  is the adjacency matrix, for example that which was introduced in Eq. (2). The initial state  $|1\rangle$  will evolve along the chain (due to the hard wall boundary conditions) with an approximate speed  $J$  (the rate at which the front of the excitation wave travels across the chain), according to the triangle wave

$$\mathcal{Q}_\Lambda = \frac{N-1}{\pi} \arcsin \left\{ \sin \left[ \pi \left( \frac{Jt}{N} - \frac{1}{2} \right) \right] \right\} + \frac{N+1}{2}. \quad (15)$$

We find that the speed  $J$  as described above is given by the derivative of Eq. (15), i.e.  $J = |\partial_t \mathcal{Q}|$  (where defined).

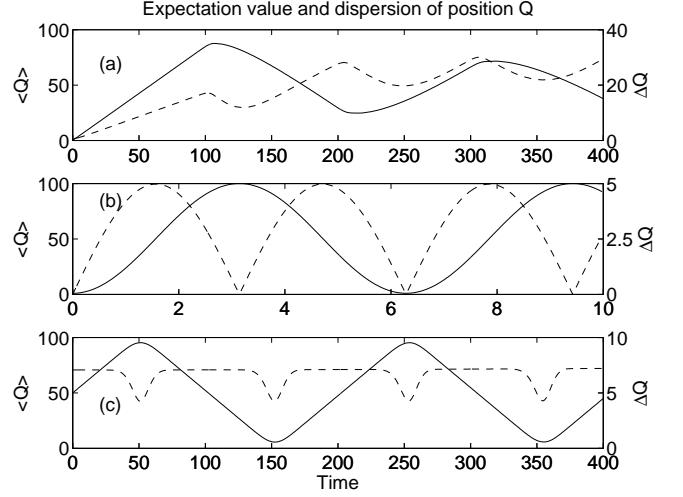


FIG. 5: Evolution of a Heisenberg spin chain Hamiltonian [Eq. (14)], with  $J = 1$ . The solid lines display the expectation value of the position  $\langle Q \rangle$ , the dashed lines show the dispersion  $\Delta Q$ . (a) Evolution of  $|1\rangle$  under uniform coupling,  $\Delta Q$  increases with time, this indicates increasing dispersion as time progresses. (b) Evolution of  $|1\rangle$  under parabolic coupling, here  $\Delta Q$  does not increase with time, as such this indicates dispersion-free evolution. (c) Evolution of a Gaussian pulse as in Eq. (26), with  $Q_c = 50$ ,  $s = 10$ ,  $k = \pi/2$ , with uniform coupling. As in (b), there is no overall increase in dispersion, as such this pulse is also dispersion-free.

By comparing Eq. (14) with Eq. (12), we see that the JCH Hamiltonian in the regime  $\Delta = 0$ ,  $\kappa \ll \beta$ , mimics two Heisenberg spin chains, in each of the photonic and the atomic states. In both cases,  $J = \kappa$  (the approximate excitation speed).

Next we consider an alternative limit, where the coupling between cavities dominates the evolution,  $\kappa/\beta \gg 1$ . In this regime, the atomic mode does not propagate at all, while the photonic mode propagates at twice the speed of the previous case. This is because the atom-photon coupling is effectively zero compared to the much faster inter-cavity coupling rate, freezing the atomic excitation. The case  $\kappa/\beta = 10^3$  is shown in Fig. (2)(e) and (f). In this limit, the Hamiltonian trivially reduces to

$$H = -\kappa A \otimes \frac{I_2 + Z}{2}, \quad (16)$$

as such, the photonic excitation travels with speed  $2\kappa$ , and the atomic excitation does not move at all. We can think of this limit as that of a pure photon gas, albeit with only one photon, which is equivalent to a single-excitation spin chain.

When  $\Delta = 0$ , and  $\kappa$  and  $\beta$  are of the same order of magnitude, the evolution of the state Eq. (11) now experiences a large amount of dispersion. This is because the evolution no longer approximates two Heisenberg spin chains (as it does in the  $\kappa/\beta \ll 1$  and  $\kappa/\beta \gg 1$  limits), but rather the full JCH nature of the evolution is ex-



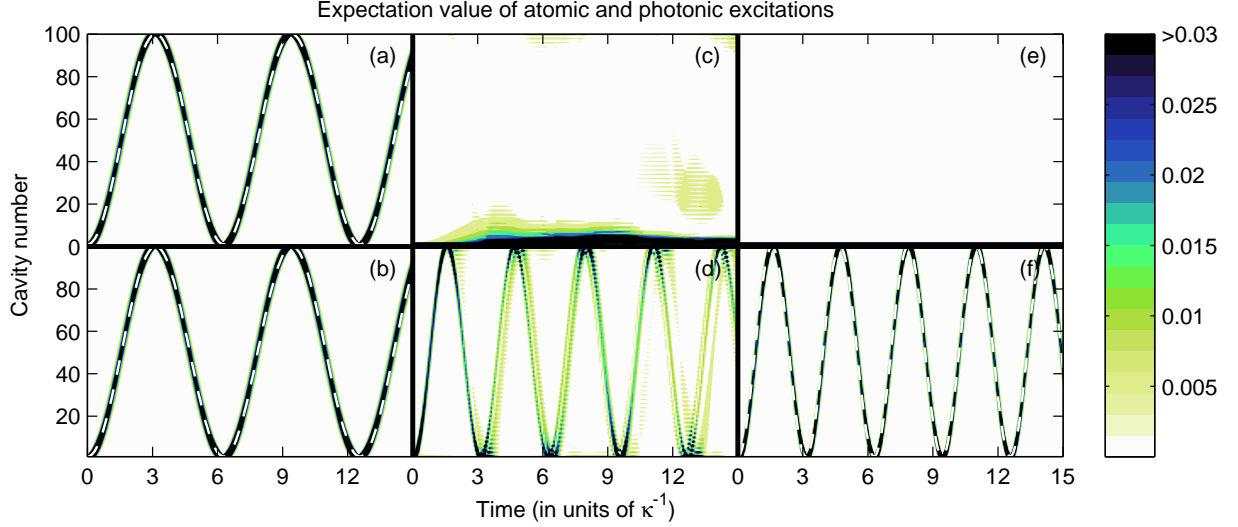


FIG. 6: (Color online) Space-time diagrams for evolution of an excitation  $(|1\rangle \otimes (|g, 1\rangle + |e, 0\rangle)/\sqrt{2})$  along a chain of 100 JC cavities with parabolic inter-cavity coupling profile. The upper plots show the population of the atomic components whereas the lower plots are the photonic components. The ratio of cavity-cavity coupling to atom-photon coupling varies from left to right, with (a) and (b)  $\kappa/\beta = 10^{-4}$ , (c) and (d)  $\kappa/\beta = 10^0$ , (e) and (f)  $\kappa/\beta = 10^3$ . In plots (a), (b) and (f), the white dashed lines represent  $\langle Q(t) \rangle$ , as given in Eq. (29). The effect of the parabolic coupling is to constrain the pulse, resulting in well defined and reversible dispersion.

pressed. As the atom-cavity coupling  $\beta$  and the cavity-cavity coupling  $\kappa$  are of the same order, there is no opportunity for the excitation to form any single cavity eigenstates, instead the excitation is relatively free to roam between photonic and atomic modes, as well as between cavities. The example  $\kappa/\beta = 10$  is shown in Fig. (2)(c) and (d).

To more clearly see this interplay between JC and photon dominated regimes, we consider the dispersion of the wave packet as it travels along the chain. Fig. (3) shows how the dispersion of a pulse changes with  $\kappa/\beta$ . We define the position operators

$$\begin{aligned} Q_{\text{photonic}} &\equiv \text{diag}(1, 0, 2, 0, \dots, N, 0) \\ Q_{\text{atomic}} &\equiv \text{diag}(0, 1, 0, 2, \dots, 0, N) \end{aligned} \quad (17)$$

in the basis  $\{|Q\rangle \otimes |g, 1\rangle, |Q\rangle \otimes |e, 0\rangle\}$ ,  $Q = 1, \dots, N$ . The definitions of Eq. (17) assume that when calculating expectation values for photonic (atomic) position, the photonic (atomic) states are selected from the wave function and normalized as a single vector of length  $N$  [34].

The dispersion for photonic and atomic modes is given by the standard deviation of the position operator  $\Delta Q$

$$(\Delta Q_{\text{type}})^2 = \langle Q_{\text{type}}^2 \rangle - \langle Q_{\text{type}} \rangle^2. \quad (18)$$

Looking at Fig. (3), we see the link between the two limits  $\kappa/\beta \ll 1$  and  $\kappa/\beta \gg 1$  for  $\Delta = 0$ . The solid (dashed) line shows  $\Delta Q_{\text{atomic}}^{\text{JCH}}$  ( $\Delta Q_{\text{photonic}}^{\text{JCH}}$ ). In these two limits, the JCH chain mimics two Heisenberg spin chains,

while in the middle range, the full JCH dynamics are realized. With increasing  $\kappa/\beta$ , the photonic (atomic) dispersion of a pulse is constant (constant) when  $\kappa/\beta \ll 1$ , increases for moderate values of  $\kappa/\beta$ , then becomes constant (zero) when  $\kappa/\beta \gg 1$ . Dispersion is measured at the time  $T = N/4\kappa$  for a system with  $N = 100$  cavities initially in the state given by Eq. (11) (i.e.  $|1\rangle \otimes |+, 1\rangle$  with  $\Delta = 0$ ). The horizontal lines drawn on the figure show the dispersion  $\Delta Q^{\text{Heis}}$  ( $Q^{\text{Heis}} = \text{diag}(1, 2, \dots, N)$ ) of a Heisenberg spin chain with 100 spins and initial state  $|1\rangle$  for  $J = \kappa$  (dotted line) and  $J = 2\kappa$  (dot-dashed line) along the excitation chain. The  $J = \kappa$  Heisenberg dispersion line matches both the photonic and atomic dispersion in the limit when  $\kappa/\beta \ll 1$ . The  $J = 2\kappa$  Heisenberg dispersion line matches the photonic dispersion in the limit when  $\kappa/\beta \gg 1$ , while the atomic dispersion in this limit tends to zero (as the atomic mode no longer propagates).

The left inset of Fig. (3) and Fig. (2)(a) and (b) correspond to the example  $\kappa/\beta = 10^{-3}$ . The inset shows the pulse profile at the time  $T = N/4\kappa$  [with pulse approximately a quarter along the chain,  $Q_{\Lambda} = N/4$ , and solid (dashed) line representing the photonic (atomic) profile], while part (a) and (b) shows that the evolution of the atomic and photonic modes are identical. The middle inset of Fig. (3) and Fig. (2)(c) and (d) correspond to the example  $\kappa/\beta = 10$ . The inset shows the high dispersion of the pulse profile at the time  $T = N/4\kappa$  (the dashed line shows atomic profile), and part (b) shows the high dispersion evolution. The right inset of Fig. (3) and Fig. (2)(e) and (f) correspond to the example  $\kappa/\beta = 10^3$ . The inset shows the pulse profile at  $T = N/4\kappa$ , note

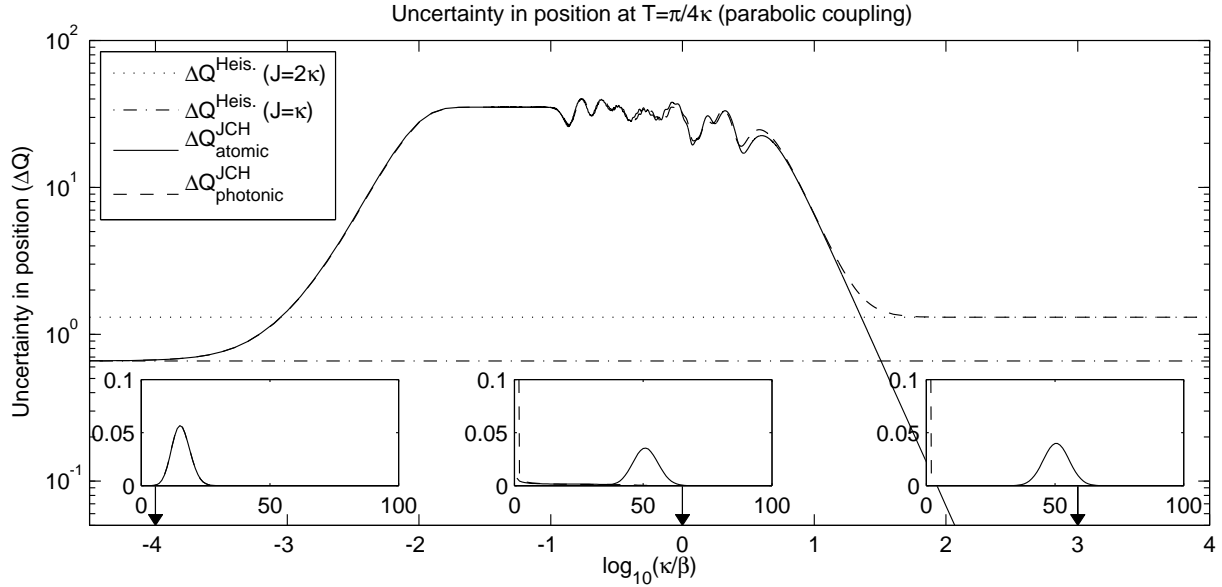


FIG. 7: Dispersion of the wave packet,  $\Delta Q$ , at a fixed point in time for a JCH system with parabolic coupling. The solid (dashed) line shows  $\Delta Q^{\text{JCH}}_{\text{atomic}}$  ( $\Delta Q^{\text{JCH}}_{\text{photonic}}$ ). The dotted (dot-dashed) line shows  $\Delta Q^{\text{Heis}}$  with  $J = 2\kappa$  ( $J = \kappa$ ). The parameter ranges are identical to Fig. (3), although the range of the vertical axis is different. The insets show the pulse profile at three values of  $\kappa/\beta$ . The solid (dashed) line represents the photonic (atomic) profile. The result is that, while the dispersion is considerably larger than the uniform coupling case, in this case the pulse is more ‘well behaved’. More precisely, the pulse has a Gaussian profile away from the boundaries and its evolution is completely reversible. In the extreme limits for  $\kappa$ , we have again perfect agreement with that expected from the appropriate spin chain model.

that the photonic profile is approximately half way along the chain ( $Q_{\Lambda} = N/2$ ), while the dashed line shows the atomic profile, which does not propagate. The atomic and photonic modes remain in superposition, despite the fact that the atomic mode does not propagate and the photonic mode does.

Consider the profile (probability distribution at an instant in time) of a single excitation as it travels along the chain. In Fig. (4)(a), we display the expectation value of the evolution of a single up spin (initially at  $|1\rangle$ ) for a Heisenberg spin chain with uniform coupling  $J$  between each of the 100 sites. One sees that the pulse is initially well-formed, but later suffers from increasing dispersion of the excitation, both when travelling through the chain, and also when reflecting from the end of the chain. Regardless, the speed of the pulse is given by  $J$ , at least for the first reflection, where the wave speed can be realistically interpreted. Fig. (5)(a) is a different way of showing the same evolution, by plotting the expectation value and uncertainty of the operator  $Q^{\text{Heis}} = \text{diag}(1, 2, \dots, N)$  highlighting the spread of the pulse with time. While the physics of Heisenberg spin chains is well studied [28, 29], it is useful to contrast this behaviour with the next regime we will examine.

### III. PARABOLIC COUPLING

One way to control the dispersion of the pulse is to define a non-uniform distribution of couplings between cavities. One such possibility is to choose a regime of parabolic couplings [26, 30], where the coupling between cavity  $i$  and cavity  $i + 1$  is given by  $\sqrt{i(N - i)}$ , so that the adjacency matrix becomes

$$A_{ij} = \begin{cases} \sqrt{j(N - j)} & i - j = 1 \\ \sqrt{i(N - i)} & j - i = 1 \\ 0 & \text{otherwise} \end{cases} \quad (19)$$

Thus the couplings will be symmetric around the central cavity (or between the two central cavities), with strongest coupling at the center of the chain and weakest coupling at the ends. A spin chain of length  $N$  with this coupling can be mapped to a single spin  $s = (N - 1)/2$  particle, placed in a magnetic field in the  $x$  direction. This system provides the physical insight for why this coupling is dispersion-free [30]. The eigenvalues of this matrix are  $E_k = N - 1 - 2k$  and the eigenvectors are

$$|k\rangle = \sum_{Q=1}^N \sqrt{\frac{(1 - N)_k (N - 1)!}{(-1)^k k! 2^{N-1} (Q - 1)! (N - Q)!}} \times K_k(Q - 1, \frac{1}{2}, N - 1) |Q\rangle, \quad (20)$$

where the Pochhammer symbol  $(N)_k$  is defined as

$$(N)_k = (N)(N+1)\dots(N+k-1), \quad k = 1, 2, 3, \dots \quad (21)$$

and the Krawtchouk polynomial  $K$  [31, 32] is related to the hypergeometric function  $F$  by

$$K_k(l, p, N) = {}_2F_1 \left( \begin{matrix} -k, -l \\ -N \end{matrix} \middle| p^{-1} \right). \quad (22)$$

Now we examine the behaviour of the JCH chain under this parabolic coupling scheme. We find that, again in the basis given by  $\{|k\rangle \otimes |g, 1\rangle, |k\rangle \otimes |e, 0\rangle\}$ , the Hamiltonian is a block diagonal matrix, with the  $k$ th block appearing as

$$\mathcal{H}_{\text{exc}}^{\text{JCH}}(k) = \begin{pmatrix} \frac{\Delta}{2} - \kappa(N-1-2k) & \beta \\ \beta & -\Delta/2 \end{pmatrix}. \quad (23)$$

The eigenvalues of the full Hamiltonian (6) in the parabolic coupling case are

$$E_{\pm}^k = \frac{1}{2} \left\{ \kappa(2k - N + 1) \pm \sqrt{[\Delta + \kappa(2k - N + 1)]^2 + 4\beta^2} \right\} \quad (24)$$

and the eigenvectors are

$$|\pm, k\rangle = \frac{(\Delta + 2E_{\pm}^k)|g, 1\rangle + 2\beta|e, 0\rangle}{\sqrt{(\Delta + 2E_{\pm}^k)^2 + 4\beta^2}} \otimes |k\rangle. \quad (25)$$

We find the matching that occurs in limiting cases for the parabolic JCH system, occurs in exactly the same way as the uniform coupling case. That is, when  $\Delta = 0$  and  $\kappa \ll \beta$ ,  $J = \kappa$  for both the atomic and photonic parts. When  $\Delta = 0$  and  $\kappa \gg \beta$ ,  $J = 2\kappa$  for the photonic mode and the atomic mode does not propagate. Figs. (6) and (7) show very similar results to Figs. (2) and (3), with only one significant difference (apart from the dispersion-free pulses), that the uncertainty in position for moderate values of  $\kappa/\beta$  is much larger than the uniform coupling case.

#### IV. GAUSSIAN PULSES

As an alternative to modifying the coupling profile, we can consider uniform coupling and a Gaussian wave packet as our initial state. In this case, the momentum distribution of the pulse is well defined (and narrow) which allows the excitation to travel down the chain with minimal increase in dispersion [17, 18]. We therefore choose an appropriate initial state

$$|\psi^{(k,s,Q_c)}(t=0)\rangle = \mathcal{N} \sum_{Q=1}^N e^{-\frac{(Q-Q_c)^2}{2s^2}} e^{-ikQ} |Q\rangle, \quad (26)$$

for a Heisenberg spin chain, or

$$\begin{aligned} & |\psi^{(k,s,Q_c)}(t=0)\rangle \\ &= \mathcal{N} \sum_{Q=1}^N e^{-\frac{(Q-Q_c)^2}{2s^2}} e^{-ikQ} |Q\rangle \otimes (|g, 1\rangle + |e, 0\rangle)/\sqrt{2}, \end{aligned} \quad (27)$$

for a JCH chain, where  $\mathcal{N}$  is the normalization,  $k$  is the wave number,  $Q_c$  is the center of the pulse,  $s$  is the width of the pulse, and  $Q$  denotes cavity number, with  $Q = 1, \dots, N$ . In this paper we choose  $Q_c = N/2$ ,  $s = N/10$ , such that the pulse is initiated at the center of the chain with a width approximately 2/10 times the length of the chain. The value  $k = \pi/2 + n\pi$ , where  $n$  is an integer, produces dispersion-free evolution of the pulse.

Fig. (8) shows the evolution of a Gaussian pulse for three different values of  $\kappa/\beta$ , in analogy to Fig. (2) and (6). The white dashed lines correspond to a triangle wave similar to Eq. (15), but with a phase shift by  $\pi/2$ . The phase shift is necessary as we have initiated the Gaussian pulse in the center of the chain, to avoid boundary effects (contrary to the first uniform coupling case, where the boundary effects were essential for the motion of the pulse). The dashed line is given by

$$Q_{\wedge}^{\text{Gaussian}} = \frac{N-1}{\pi} \arcsin \left[ \sin \left( \frac{J\pi t}{N} \right) \right] + \frac{N+1}{2}. \quad (28)$$

In the limits  $\kappa/\beta \ll 1$  and  $\kappa/\beta \gg 1$ , the Gaussian pulse with the choice of  $k = \pi/2$  evolves under simple translation motion, interrupted by reflection off the boundaries. This translational motion, as well as the interference pattern as it reflects off the boundary, mimics exactly the propagation of a Gaussian wave packet under the one-dimensional Schrödinger equation [17, 18, 33].

Fig. (9) shows the dispersion of the pulse as a function of  $\kappa/\beta$ , in analogy to Fig. (3) and (7). Note how this figure is much simpler than the earlier two, as the dispersion is a constant throughout the evolution of the pulse, provided the pulse is not interacting with the boundaries. As such, only one horizontal line to indicate dispersion of a corresponding Heisenberg spin chain is necessary. Also, the dispersion of the photonic mode is equal to the dispersion of the atomic mode.

By comparing Fig. (4)(a) (uniform coupling) with (4)(b) (parabolic coupling) and Fig. (4)(c) (uniform coupling, Gaussian pulse) we can indeed see that the pulse in the uniform chain has more dispersion than that of the parabolic chain and the uniform chain with an initial Gaussian pulse, the dispersion is manifest as a number of faint lines parallel to the main wavefront. Further, in Fig. (5) we have plotted the expectation value of the position  $\langle Q \rangle$  (solid lines) and  $\Delta Q$  (dashed lines), for both the uniform coupling (a), parabolic coupling (b) and uniform coupling with Gaussian pulse (c) cases. In fact, the expectation value of the position  $Q$  in the parabolic chain is of this simple form:



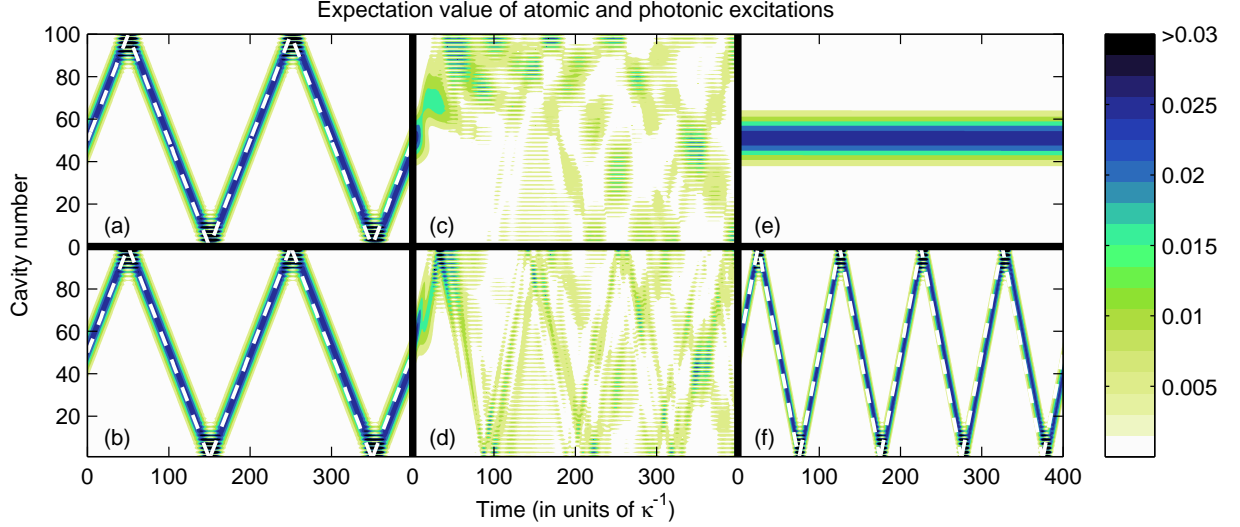


FIG. 8: (Color online) Space-time diagrams for evolution of an Gaussian pulse along a chain of 100 JC cavities with a uniform inter-cavity coupling profile. The upper plots show the population of the atomic components whereas the lower plots are the photonic components. The ratio of cavity-cavity coupling to atom-photon coupling varies from left to right, with (a) and (b)  $\kappa/\beta = 10^{-2}$ , (c) and (d)  $\kappa/\beta = 10^0$ , (e) and (f)  $\kappa/\beta = 10^3$ . In plots (a), (b) and (f), the white dashed lines represent  $Q_{\Lambda}^{\text{Gaussian}}$ , as given in Eq. (28). The effect of the Gaussian pulse is to have chosen a narrow momentum distribution, which allows the excitation to propagate freely in the system.

$$\langle Q(t) \rangle = \frac{1}{2}[N + 1 - (N - 1) \cos Jt]. \quad (29)$$

Hence the period of oscillation is  $2\pi/J$ , which does not depend on the number of cavities  $N$ . For the coupling profile, we find that the pulse (while more dispersed) is approximately Gaussian shaped in space. This can be seen by examining Fig. (10)(b), which shows the pulse profile at fixed instants in time. In comparison, Fig. (10)(a) has much higher dispersion, while Fig. (10)(c) also has low dispersion, which is largely constant and only reduces slightly as the pulse is reflected at the boundaries of the chain.

## V. LARGE DETUNING LIMIT

We now consider the case where the magnitude of the detuning is much larger than the other energy scales of the system, that is,  $\kappa, \beta \ll |\Delta|$ . The effect of increasing detuning is to *decrease* the atom-photon coupling, thereby approximating a Bose-Hubbard system. We are therefore interested in any non-trivial effects which appear in this limit.

We now shift again to an interaction picture, where states of the system  $|\psi\rangle$  are transformed to

$$|\xi\rangle = e^{i(\Delta I \otimes Z/2 + \beta I \otimes X)t} |\psi\rangle. \quad (30)$$

Under this shift, the Hamiltonian becomes

$$H = -\kappa A \otimes \left[ \frac{I+Z}{2} \left( 1 - \frac{2\beta^2}{\Delta^2 + 4\beta^2} \right) + \frac{I-Z}{2} \frac{2\beta^2}{\Delta^2 + 4\beta^2} + \frac{\Delta\beta}{\Delta^2 + 4\beta^2} X \right]. \quad (31)$$

In this equation, the coefficient of  $(I+Z)/2$  is related to the speed of the atomic component, and the coefficient of  $(I-Z)/2$  is related to the speed of the photonic component. We will discuss the effect of the  $X$  term shortly.

To explore the dynamics of this system, we again start with the equal superposition initial state as given in Eq. (11). For example, the uniform coupling case with  $\Delta = 10^3\beta$ ,  $\kappa = \beta$  is shown in Fig. (11)(a). By again comparing to the Heisenberg spin chain Hamiltonian, Eq. (14), we see now that the photonic excitation corresponds to a Heisenberg spin chain with speed  $J = 2\kappa[1 - 2\beta^2/(4\beta^2 + \Delta^2)]$ , and the atomic excitation corresponds to a Heisenberg spin chain with speed  $J = 2\kappa\beta^2/(4\beta^2 + \Delta^2)$ . In this regime, the atomic and photonic excitations travel at two completely different speeds: the photonic mode travels much faster than the atomic mode, although the integrity of each mode is preserved. We also can see in Fig. (11) that this splitting of the system into two separate modes happens for both parabolic coupling (b) and an initial Gaussian pulse (c). This splitting is an observation which can be predicted directly from the  $\kappa A$  independent form of the various components of Eq. (31). Note that the final term of Eq. (31) is significantly different from both the time scale of the photonic propagation ( $\approx 2\kappa$ ) and the time scale of the

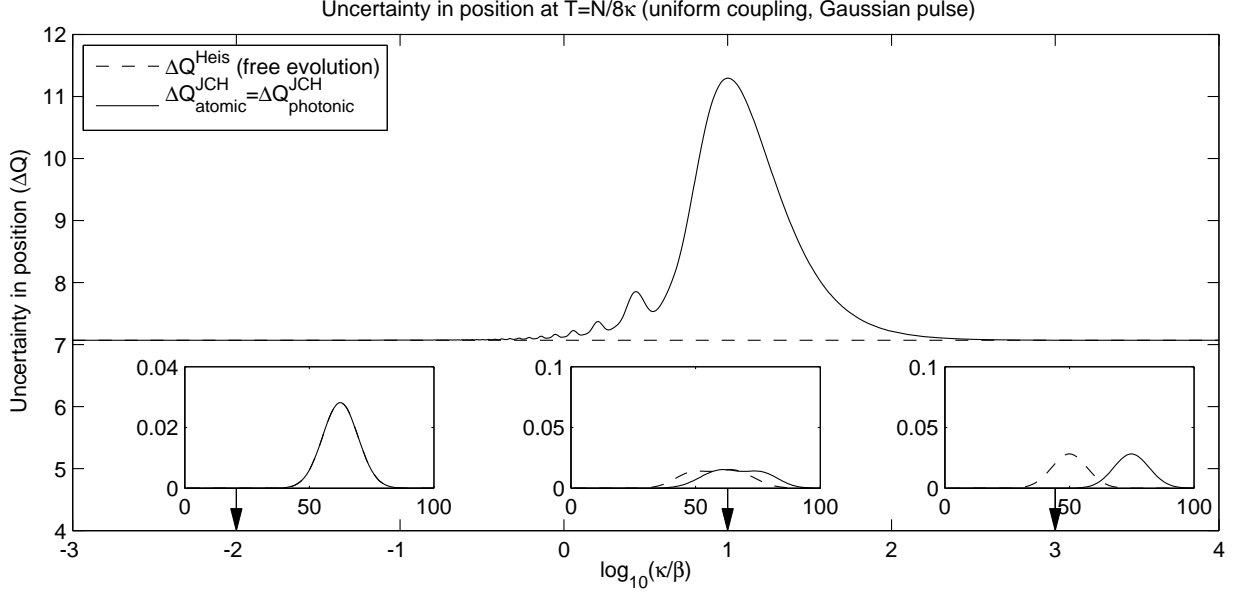


FIG. 9: Dispersion of a Gaussian wave packet,  $\Delta Q$ , at a fixed point in time, as a function of  $\kappa/\beta$ , at  $\Delta = 0$ . The dispersion is measured at time  $T = N/8\kappa$ , at which point the packet is ‘freely’ evolving along the chain. The initial state of the Gaussian is given by Eq. (27), with center of the pulse at  $Q_c = N/2$ , width of the pulse  $s = N/10$ , wave number  $k = \pi/2$ , and number of cavities  $N = 100$ . The width of the pulse is small enough such that the boundaries do not have an effect on  $\Delta Q$  for the value of  $T = N/8\kappa$  in the limits  $\kappa/\beta \ll 1$  and  $\kappa/\beta \gg 1$ . At the left of the plot,  $\kappa/\beta \ll 1$ , and the JCH chain mimics two identical Heisenberg spin chains, an example is shown of this localized behavior in Fig. (8)(a) and (b), where  $\kappa/\beta = 10^{-2}$ . The corresponding spatial profile of the pulse is shown in the left inset, (the solid line shows the photonic profile and the dashed line shows the atomic profile, in this case they are coincident). At the right of the plot  $\kappa/\beta \gg 1$ , and the photonic mode of the JCH chain mimics a Heisenberg spin chain, while the atomic mode does not propagate at all. An example of this type of localized behavior is shown in Fig. (8)(e) and (f), where  $\kappa/\beta = 10^3$ , the corresponding profile of the pulse at  $T = N/8\kappa$  is shown in the right inset. In the middle of the plot a travelling excitation shows a large amount of dispersion, an example of this delocalized behavior is shown in Fig. (8)(c) and (d), where  $\kappa/\beta = 10$ , and the corresponding profile at  $T = N/8\kappa$  is shown in the middle inset. The horizontal line shows the dispersion  $\Delta Q^{\text{Heis}}$  of a freely evolving pulse [this value does not change, provided the pulse is not interacting with the boundary, as is evidenced by Fig. (5)(c)].

atomic propagation ( $\approx 2\kappa\beta^2/\Delta^2$ ). As such it does not contribute significantly to either mode of propagation in the very large detuning limit.

If the detuning is reduced such that this separation of time scales is not so strong, we must ask the question what is the effect of this final  $X$  term in Eq. (31)? To answer this, we write it out in the original basis of atoms and photons on neighboring sites  $j$  and  $j + 1$ ,

$$X_{j,j+1} = \sigma_j^+ a_{j+1} + \sigma_j^- a_{j+1}^\dagger + \sigma_{j+1}^+ a_j + \sigma_{j+1}^- a_j^\dagger, \quad (32)$$

in which we see that it is an effective JC type coupling between neighboring atoms and photons. The effect of this term on the propagating atom and photon chains will be zero at first order as it couples *between* chains. The second order effect is not zero, as

$$[X_{j,j+1}, X_{j+1,j+2}] = -(\sigma_j^+ \sigma_{j+2}^- - \sigma_{j+2}^+ \sigma_j^- + a_j^\dagger a_{j+2} - a_{j+2}^\dagger a_j), \quad (33)$$

giving an effective next-nearest-neighbor coupling (assuming the one excitation subspace). The strength of

this correction is given by the square of the  $A \otimes X$  coefficient in Eq. (31) and therefore vanishes as the detuning is increased. In the limit where mixing effects are visible due to this additional term, we also observe asymmetric behavior with respect to the sign of the detuning, similar to that seen previously in a two cavity system [8]. It should be noted that here, we always initialize the system in an equal superposition of atomic and photonic states, whereas in previous work, the detuning asymmetry is accentuated by an initial state which is always an eigenstate of the JC Hamiltonian.

## VI. CONCLUSIONS

In conclusion, we find that when limited to the one excitation subspace, one can analytically solve for the evolution of the excitation pulse. As such, we extend previous work on the topic [8, 9] from  $N = 2$  to the many-cavity regime. We observe both localized and delocalized behavior in this system, which points to a complex interplay between atomic and photonic degrees of

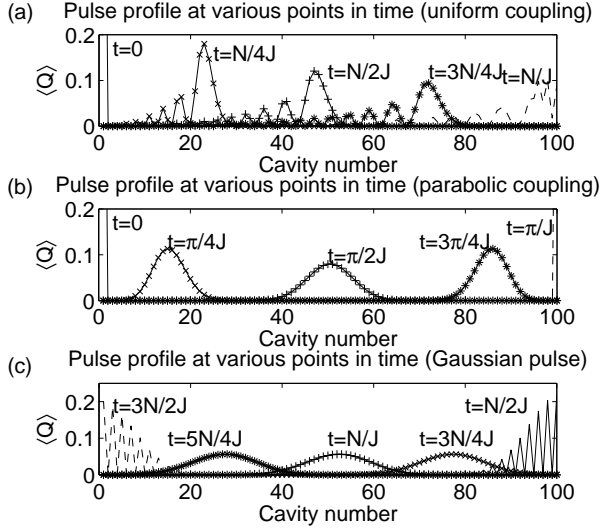


FIG. 10: The pulse profile for various points in time as a function of cavity number, for evolution of a Heisenberg spin chain. (a) Evolution of  $|1\rangle$  with uniform coupling between spins. (b) Evolution of  $|1\rangle$  with parabolic coupling between spins. (c) Evolution of a Gaussian pulse, as given in Eq. (26) with uniform coupling between spins. In the first uniform case, the profile is initially given by a Kronecker delta function, but later spreads into a function with one primary peak and a number of smaller trailing peaks. In the parabolic case, at each end of the chain, the pulse is given by a Kronecker delta function, while in the middle of the chain the pulse approximates a Gaussian. In the uniform coupling case with an initial Gaussian pulse, it evolves along the chain with fixed profile, and at the ends of the chain interferes and changes direction.

freedom, even in the single excitation limit.

We consider three natural limits, and show that the behaviour of the atomic and photonic modes of the JCH chain can be mapped to two independent Heisenberg spin chains. In the limit when the detuning is zero and the inter-cavity coupling is much smaller than the atom-photon coupling, we find that the system is mapped to two Heisenberg spin chains both with  $J = \kappa$ . When the detuning is zero but atom-photon coupling is much smaller than inter-cavity coupling, the photonic mode propagates with approximate speed  $J = 2\kappa$  and the atomic mode does not.

In the limit when the detuning is much larger than both the inter-cavity coupling and the atom-photon coupling, the system is mapped to two Heisenberg spin chains, with  $J = 2\kappa[1 - 2\kappa\beta^2/(\Delta^2 + 4\beta^2)]$  for the photonic mode, and  $J = 2\kappa\beta^2/(\Delta^2 + 4\beta^2)$  for the atomic mode. We also derive similar analytic solutions for the case of a parabolic variation in inter-cavity coupling, resulting in a Gaussian like wave packet propagation along the chain, as well as an initial Gaussian pulse in a uniform coupled chain.

The JCH system provides an interesting playground for studying many-body physics in an atom photon con-

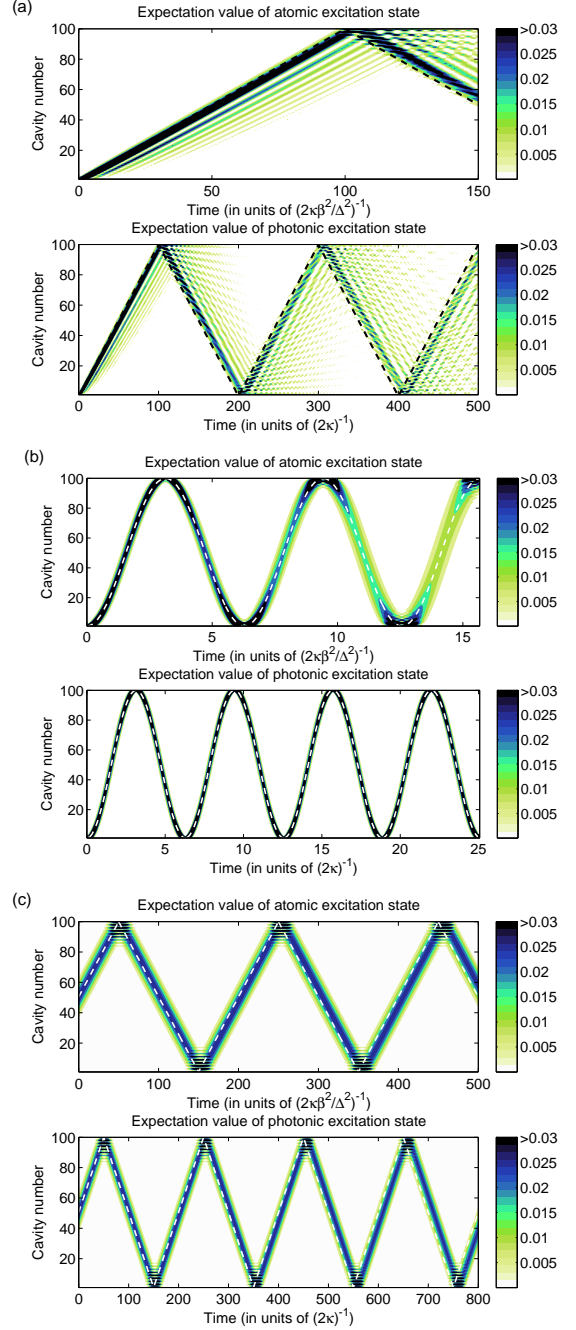


FIG. 11: (Color online) These plots show the evolution of the state  $|1\rangle \otimes (|e, 0\rangle + |g, 1\rangle)$  (a) and (b) and a Gaussian pulse (c) in a one-dimensional JCH system consisting of 100 cavities, with  $\kappa = \beta$  and  $\Delta/\beta = 10^3$ . Note the time scales are different in each case. (a) Evolution in a uniform chain, where the dashed lines are a triangle wave giving approximate evolution of the wavefront, as given in Eq. (15). (b) Evolution in a parabolically coupled chain, where the dashed lines are as given in Eq. (29). (c) Evolution in a uniformly coupled chain, with an initial Gaussian pulse, as given in Eq. (27). The dashed lines show the expectation value of position, as given in Eq. (28).

text. Given that initial experiments will be limited in both cavity and excitation number, it is important we understand these temporal dynamics in a range of system size regimes.

## VII. ACKNOWLEDGEMENTS

M.M. wishes to thank Dr. Brendon Lovett for useful discussions. J.H.C. wishes to acknowledge the support

of the Alexander von Humboldt foundation. A.D.G. and L.C.L.H. acknowledge the Australian Research Council for financial support Projects No. DP0880466 and No. DP0770715, respectively. This work was supported by the Australian Research Council, the Australian Government, and the US National Security Agency (NSA) and the Army Research Office (ARO) under contract number W911NF-08-1-0527.

- 
- [1] I. Bloch, Nat. Phys. **1**, 23 (2005).
  - [2] R. Balili, V. Hartwell, D. Snoke, L. Pfeiffer, and K. West, Science **316**, 1007 (2007).
  - [3] M. J. Hartmann, F. G. S. L. Brandão, and M. B. Plenio, Nat. Phys. **2**, 849 (2006).
  - [4] A. D. Greentree, C. Tahan, J. H. Cole, and L. C. L. Hollenberg, Nat. Phys. **2**, 856 (2006).
  - [5] D. G. Angelakis, M. F. Santos, and S. Bose, Phys. Rev. A **76**, 031805(R) (2007).
  - [6] D. Rossini and R. Fazio, Phys. Rev. Lett. **99**, 186401 (2007).
  - [7] S. Bose, D. G. Angelakis, and D. Burgath, Journ. of Mod. Opt. **54**, 2307 (2007).
  - [8] E. K. Irish, C. D. Ogden, and M. S. Kim, Phys. Rev. A **77**, 033801 (2008).
  - [9] C. D. Ogden, E. K. Irish, and M. S. Kim, Phys. Rev. A **78**, 063805 (2008).
  - [10] J. Koch and K. L. Hur, arXiv:0905.4005 (2009).
  - [11] N. Na, S. Utsunomiya, L. Tian, and Y. Yamamoto, Phys. Rev. A **77**, 031803(R) (2008).
  - [12] M. Grochol, Phys. Rev. B **79**, 205306 (2009).
  - [13] A. Wallraff, D. I. Schuster, L. Frunzio, R. S. Huang, J. Majer, S. Kumar, S. M. Girvin, and R. J. Schoelkopf, Nature **431**, 162 (2004).
  - [14] A.-C. Ji, Q. Sun, X. C. Xie, and W. M. Liu, Phys. Rev. Lett. **102**, 023602 (2009).
  - [15] D. Gerace, H. Türeci, A. Imamoglu, V. Giovannetti, and R. Fazio, Nat. Phys. **5**, 281 (2009).
  - [16] M. Trupke, E. A. Hinds, S. Eriksson, E. A. Curtis, Z. Moktadir, E. Kukharenya, and M. Kraft, Appl. Phys. Lett. **87**, 211106 (2005).
  - [17] J.-T. Shen and S. Fan, Phys. Rev. Lett. **95**, 213001 (2005).
  - [18] J.-T. Shen and S. Fan, Optics Letters **30**, 2001 (2005).
  - [19] M. I. Makin, J. H. Cole, C. Tahan, L. C. L. Hollenberg, and A. D. Greentree, Phys. Rev. A **77**, 053819 (2008).
  - [20] M. Paternostro, G. S. Agarwal, and M. S. Kim, New J. Phys. **11**, 013059 (2009).
  - [21] J. Lu, L. Zhou, L.-M. Kuang, and C.P. Sun, Phys. Rev. E **79**, 016606 (2009).
  - [22] H. Altug and J. Vučković, Appl. Phys. Lett. **86**, 111102 (2005).
  - [23] D. C. Mattis, ed., *The Many-Body Problem* (World Scientific, Singapore, 1993).
  - [24] S. Sachdev, *Quantum phase transitions* (Cambridge University Press, Cambridge, 1999).
  - [25] E. T. Jaynes and F. W. Cummings, in *Proc. of the IEEE* (1963), vol. 51, p. 89.
  - [26] M. Christandl, N. Datta, A. Ekert, and A. J. Landahl, Phys. Rev. Lett. **92**, 187902 (2004).
  - [27] M. Nielsen and I. Chuang, *Quantum Computation and Information* (Cambridge University Press, 2000), 2nd ed.
  - [28] M. P. A. Fisher, P. B. Weichman, G. Grinstein, and D. S. Fisher, Phys. Rev. B **40**, 546 (1989).
  - [29] H. E. Stanley, Phys. Rev. **179**, 570 (1969).
  - [30] C. Albanese, M. Christandl, N. Datta, and A. Ekert, Phys. Rev. Lett. **93**, 230502 (2004).
  - [31] A. N. Atakishiev, E. Jafarov, S. Nagiyev, and K. Wolf, Revista Mexicana de Fisica **44**, 235 (1998).
  - [32] W. Al-Salam, *Orthogonal Polynomials: Theory and Practice* (Kluwer Academic, Dordrecht, 1990).
  - [33] M. A. Doncheski and R. W. Robinett, Eur. J. Phys. **20**, 29 (1999).
  - [34] Imagine measuring two qualities on each of an infinite set of identically prepared 1D JCH systems. The first quality is the atomic/photonic nature of the excitation. The second quality is position. Averaging the position reading of all photonic (atomic) systems gives the expectation value of the photonic (atomic) position, as given in Eq. (17).